crystals

MDPI

Article

Study on Creep Damage in $Sn_{60}Pb_{40}$ and $Sn_{3.8}Ag_{0.7}Cu$ (Lead-Free) Solders in c-Si Solar PV Cell Interconnections under In-Situ Thermal Cycling in Ghana

Frank Kwabena Afriyie Nyarko [1,*], Gabriel Takyi [1] and Francis Boafo Effah [2]

[1] Department of Mechanical Engineering, College of Engineering, Kwame Nkrumah University of Science and Technology, Kumasi, Ghana; gabrieltakyi@yahoo.co.uk
[2] Department of Electrical and Electronic Engineering, College of Engineering, Kwame Nkrumah University of Science and Technology, Kumasi, Ghana; fbeffah.coe@knust.edu.gh
* Correspondence: fnyarko.coe@knust.edu.gh

Abstract: A numerical study on the creep damage in soldered interconnects in c-Si solar photovoltaic cells has been conducted using equivalent creep strain, accumulated creep strain and accumulated creep energy density methods. The study used data from outdoor weathering of photovoltaic (PV) modules over a three-year period (2012–2014) to produce temperature cycle profiles that served as thermal loads and boundary conditions for the investigation of the soldered interconnects' thermo-mechanical response when exposed to real-world conditions. A test region average (TRA) temperature cycle determined in a previous study for the 2012–2014 data was also used. The appropriate constitutive models of constituent materials forming a typical solar cell were utilized to generate accurate material responses to evaluate the damage from the thermal cycles. This study modeled two forms of soldered interconnections: Sn60Pb40 (SnPb) and Sn3.8Ag0.7Cu (Pb-free). The results of the damage analysis of the interconnections generated from the thermal cycle loads using accumulated creep strain method showed that the Pb-free solder interconnection recorded greater damage than that of the SnPb-solder interconnection for the TRA, 2012, 2013 and 2014 temperature cycles. The percentage changes from SnPb to Pb-free were 57.96%, 43.61%, 44.87% and 45.43%, respectively. This shows significant damage to the Pb-free solder under the TRA conditions. Results from the accumulated creep energy density (ACED) method showed a percentage change of 71.4% (from 1.3573×10^5 J/mm^3 to 2.3275×10^5 J/mm^3) in accumulated creep energy density by replacing SnPb-solder with Pb-free solder interconnection during the TRA thermal cycle. At the KNUST test site in Kumasi, Ghana, the findings show that Sn60Pb40 solder interconnections are likely to be more reliable than Pb-free solder interconnections. The systematic technique employed in this study would be useful to the thermo-mechanical reliability research community. The study also provides useful information to PV design and manufacturing engineers for the design of robust PV modules.

Keywords: strain damage; interconnections; accumulated creep energy density; thermal cycles

Citation: Afriyie Nyarko, F.K.; Takyi, G.; Effah, F.B. Study on Creep Damage in $Sn_{60}Pb_{40}$ and $Sn_{3.8}Ag_{0.7}Cu$ (Lead-Free) Solders in c-Si Solar PV Cell Interconnections under In-Situ Thermal Cycling in Ghana. *Crystals* **2021**, *11*, 441. https://doi.org/10.3390/cryst11040441

Academic Editor: Ing. José L. García

Received: 22 February 2021
Accepted: 8 April 2021
Published: 19 April 2021

1. Introduction

The world's energy is going through a transformation from being heavily reliant on fossil fuels to being reliant on renewable resources. Furthermore, renewable energy has been targeted in the quest to delay or even stop the major challenges of climate change and global warming [1]. The world's photovoltaic installed capacity steadily grew from 135 GW in 2013 to 480 GW by the end of 2018, rising 3.5-fold over five years.

With the development of solar cell structure design, micro-nano laser precision machining, and other technologies, the cost per kilowatt of photovoltaic power generation has decreased [2]. However, one key concern that remains unresolved in the PV industry is the degradation of field-installed modules.

According to King [3], field modules undergo regular temperature swings of around 60 °C (maximum). Temperature fluctuations result in the initiation and progression of fatigue cracks in the solder interconnection. This is caused by a mismatch in the thermal expansion coefficients (CTE) of silicon, glass, copper and solder when they are bonded together. There are two types of CTE mismatches: local and global. Clech [4] clarified that when solder joints are stressed and deformed to accommodate the effect of CTE mismatch from surrounding component materials such as cells, glass and interconnect, global CTE mismatch occurs. In addition, local CTE mismatch occurs when the solder material's expansion is limited by the material to which it is soldered. The development of microcracks is one of the results of solder joint deterioration. An open circuit will result if a crack spreads across the entire joint region. An open circuit increases the electrical resistance across the solder joint. As a result, this phenomenon has a substantial effect on the production capacity of c-Si solar PV modules (PVMs). Since power loss is linked to increasing series resistance (Rs) in the form I^2R_s [5,6], high-current PV modules are particularly affected.

When the temperature of the solder rises, it creeps. At high homogeneous temperatures, such as those found in tropical climates [7], the creep response is important. Grain boundary sliding (GBS) and matrix creep (MC) are two factors that contribute to solder creep. It has been discovered that the latter has a more destructive creep function, resulting in a shorter joint life. Clech [4] further indicated that the creep mechanism is temperature- and stress-dependent and that it increases as the strain rate/deformation increases. The formation of a brittle intermetallic compound (IMC) layer in c-Si PVMs is a result of a soldered tin-containing interconnection. On one side, the IMC layer is formed between the solder and the copper ribbon interface, and, on the other side, it is formed between the solder and the silver fingers. Cu_3Sn_5 or Ag_3Sn grains suspended in a solder matrix make up the IMC. The resulting thermo-mechanical stress causes a change in the microstructure of the IMC layer in the solder joint during thermal cycling of the PV module (coarsening and thickening). As a result, this layer is vulnerable to crack initiation and propagation. For high-temperature operations, this effect is important.

Research into solar PV reliability is continuous, with several reported studies, such as in [8–18]. However, some of the shortcomings identified include the over-simplification of the constitutive behaviors of the constituent materials forming the solar cell as well as the non-inclusion of intermetallic compound (IMC) layers in solder interconnect geometry. In their thermo-mechanical assessment of encapsulated solar cells, Dietrich et al. [11] modeled the solder interconnection as "interconnection paste," ignoring the existence of IMCs. Similarly, Wiese et al. [12,13], in investigating the constitutive behavior of copper ribbons, modeled silicon and silver materials in the cell as linear elastic in addition to ignoring the presence of IMCs. Furthermore, Chen et al. [14] investigated the residual stress and bow induced by soldering in the silicon cell interconnect by modeling all cell materials as temperature-independent elastic, perfectly plastic. Eitner et al. [16,17], in the investigation of thermal stresses and strains in solar cells, and Hasan et al. [8,18], in the finite element analysis and life prediction of solar PV modules, used material constitutive models derived from experimental testing that accurately describe the true mechanical properties of various solar cell materials. However, the model used in their investigation did not include a solder with its IMCs. In the case of Hasan et al. [8,18], the model was simplified further to exclude solder interconnection. On the other hand, Zarmai et al. [19] performed an optimization study on solder interconnects in PV modules using the Taguchi method. The Cu3Sn5 IMC layer was included in the geometric model used for the analysis, but the Ag3Sn IMC layer was not. Furthermore, except for the solder, which showed creep, the study used linear elastic models to predict the constitutive behavior of all laminating materials.

The absence of IMCs in these experiments, according to the studies examined, may result in inaccurate simulation results. For tin-based solder alloys and metallized copper bond pads, IMC formation in solder joint interfaces is well-known. Another reason that researchers avoid using IMCs in simulations is the large number of mesh elements and

nodes produced, which necessitates the use of a high-performance computer (HPC) for a numerical solution. HPCs with superior processing power and material property data are now available for the IMCs, thanks to recent technical developments and materials engineering studies. The over-simplification of material behavior and cell geometry has led to discrepancies in reported modeling results. In addition, for thermal cycling research, most modeling studies used the International Electrotechnical Commission qualification test standard (IEC 61215) conditions. The PV modules' real field module temperature cycles (which are location-dependent) receive very little attention.

All constituent materials, as well as the solder and its derivative IMC layers, were included in the three-dimensional geometric models of the c-Si solar cell (cell-to-cell interconnection) in this study. The thermo-mechanical response of the cell to field temperature cycles created from in-situ climatic conditions in a Sub-Saharan Africa environment (Kumasi, Ghana) was then simulated using a finite element analysis (FEA) program (ANSYS v 18.2). Furthermore, the creep damage in solder joints for both Sn60Pb40 and Sn3.8Ag0.7Cu alloys was analyzed using simulation results from field temperature cycles.

2. Materials and Methodology

2.1. Test Rig for Data Collection and Generation of Test Region Thermal Cycle Profile

Figure 1 shows the rig for monitoring the outdoor climate used for this study. The rig contains other types of crystalline silicon PV modules. However, only the mono-crystalline modules were used for this investigation. Figure 2 presents the monitoring station that was used for the data collection. The rigs are located at the College of Engineering KNUST, Kumasi, Ghana. The system was installed in 2012 with financial assistance from the World Bank through the Africa Renewable Energy Access programme (AFREA) under the project title, Capacity Upgrading for West African Partners in Renewable Energy Education. The site location (College of Engineering, KNUST, Kumasi, Ghana) is latitude 6°40" N and longitude 1°37" W, at an elevation of 250 m above sea level.

The modules are unshaded and mounted on an inclined rooftop with a tilt angle of 5°, and oriented toward the equator (southwards). Furthermore, a 4 kW Sunny Boy DC-AC inverter (SB 3800), manufactured by System, Mess and Anlagentechnik (SMA) in Niestetal, Germany connects each of the various PV module technologies to the grid. There are five inverters connected and integrated to communicate with a SMA Sunny WebBox via a Bluetooth ad-hoc connection. The SMA Sunny WebBox transmitted and stored the data output from the PV systems on a dedicated server. Additionally, an SMA Sunny portal was created on the dedicated server from the University network to provide an online monitoring system. Calibrated platinum sensors (PT100) manufactured by TC Limited in Uxbridge, United Kingdom with measurement accuracy of $\pm$0.5 °C, resolution of 0.1 °C positioned at the center of each module (on the backside) measured the module temperatures. The data logged include environment temperature, total insolation, module temperature, operating current and voltage, wind speed and total output power.

The data were collected at 5-min intervals between the periods of March 2012 and December 2014. The study and data analysis were limited to the mono-crystalline PV-modules.

The study used four temperature load profiles (2012, 2013 and 2014) and test region average (TRA) thermal cycles created from three years of real-time monitoring of installed PV modules at the test site. In a previous study [20], the methodology for producing these temperature profiles was extensively discussed.

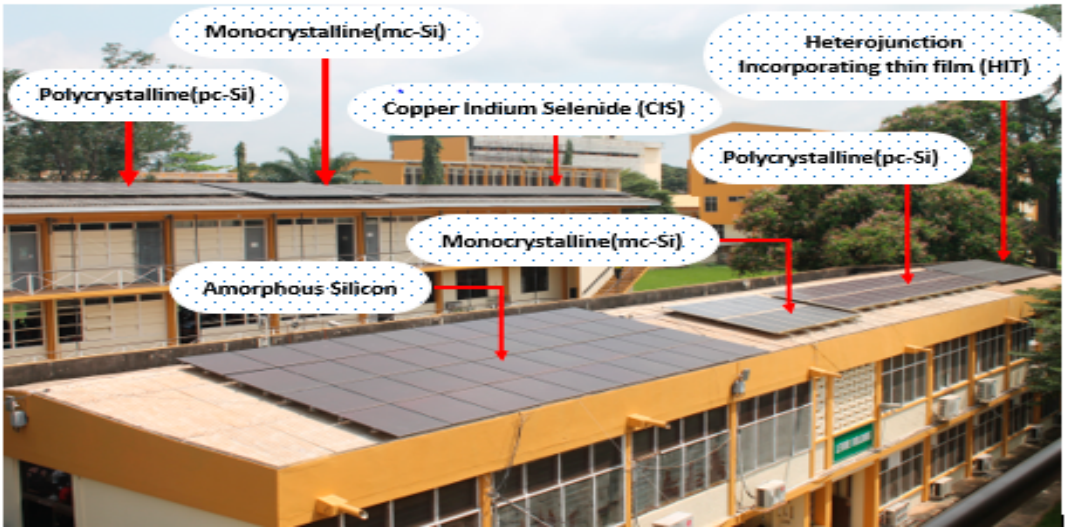

Figure 1. Outdoor monitoring set-up at College of Engineering KNUST, Kumasi, Ghana.

Figure 2. Monitoring station for outdoor test set-up at College of Engineering KNUST, Kumasi, Ghana.

2.2. Thermal Loads and Boundary Conditions

Figure 3 and Table 1 summarize the results of temperature cycle profiles generated from the real time outdoor weathering of the PV modules. The profiles show extended dwell times as well as overall cycle time. A typical daily cycle time is completed in 86,400 s (24 h).

As shown in Table 1, the mean daily temperature gradients for the generated cycles are relatively smaller when compared with the IEC 61215. A maximum of 40.2 °C was recorded in 2012, whereas the IEC 61215 temperature gradient is 125 °C.

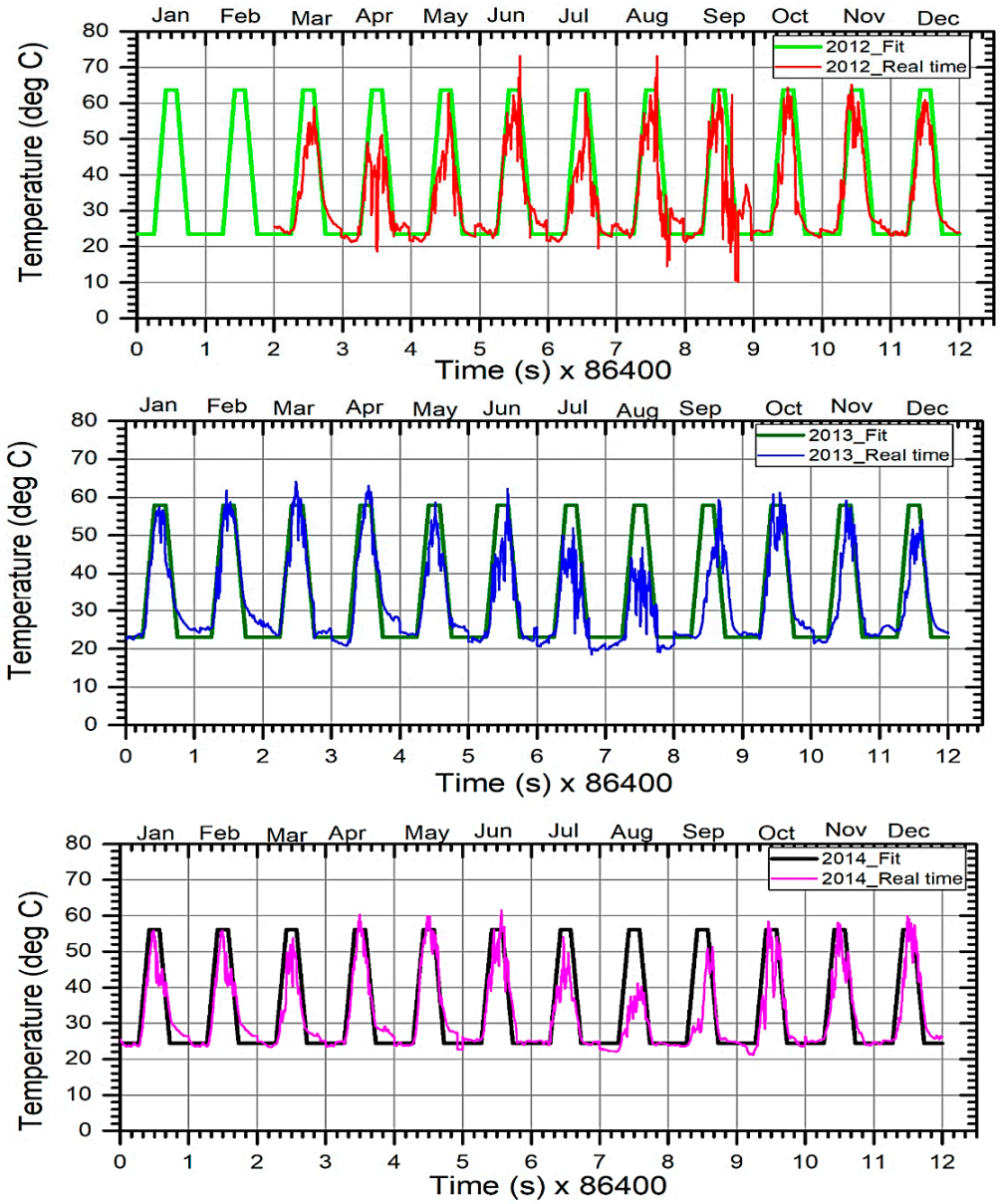

Figure 3. In-situ thermal cycle profiles fitted onto real-time module temperature profile for 2012–2014 [20].

The summary of the critical parameters presented in Table 1 shows that the effect of the employment of IEC 61215 on the thermo-mechanical degradation qualification of the c-Si PV module is likely to be significantly different from the generated temperature cycles.

Table 1. Thermal loads and boundary conditions from field thermal cycling [20].

Test Year		2012	2013	2014	TRA	IEC 61215
Dwell time (min)	Mean hot dwell	212	225	219	218.7	10
	Mean cold dwell	359	357	390	368.7	10
Ramp rate (deg/min)	Mean. ramp rate	9.51	8.65	8.82	8.996	100
Mean module hot dwell temperature (HDT)/deg.		63.7	57.9	56.1	58	85
Mean module cold dwell temperature (CDT)/(deg.)		23.5	23	24.4	23.7	−40
Temperature gradient		40.2	34.9	31.7	34.3	125

2.3. Solar Cell Materials and Properties

Figure 4 presents the architecture of a conventional c-Si PV cell interconnection. The conventional cell-to-cell interconnection architecture of a c-Si PV module involves connecting solder-coated copper (Cu) ribbons in a series arrangement. The ribbons connect the silver (Ag) electrodes deposited in the silicon crystal via solder bonds. These materials forming the interconnections (Ag-finger-solder-IMCs-copper ribbon) of the module have different co-efficients of thermal expansion (CTE). Park et al. [21] explain that the variation in the CTE of constituent materials bonded together to form the module induces thermo-mechanical stresses. Consequently, load effects from temperature cycling culminate in the initiation and development of fatigue cracks in the solder interconnection.

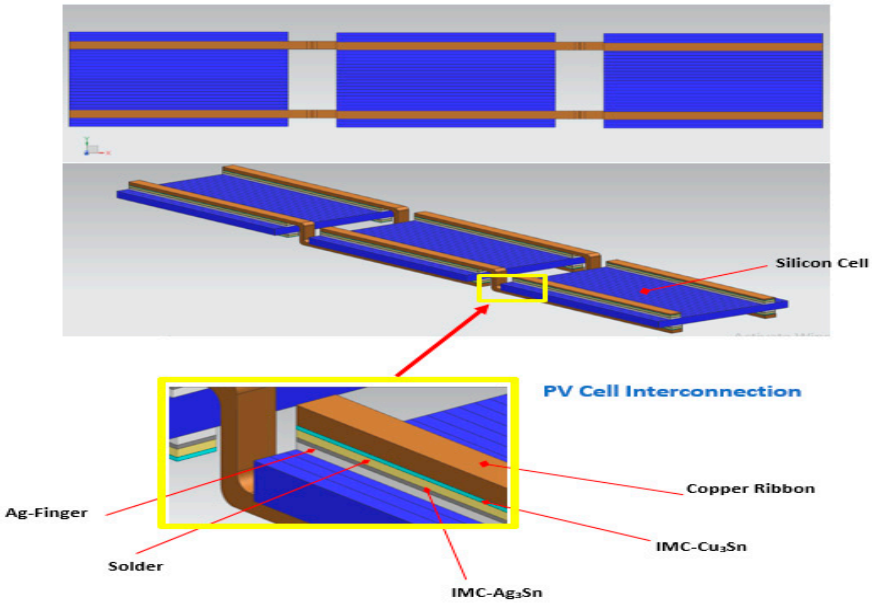

Figure 4. Conventional front-to-back cell interconnection technology in c-Si PV module.

Geometric models of solar cells were interconnected in this study using two separate solder formulations as interconnecting materials, namely Pb60Sn40 and Sn3.8Ag0.7Cu. Table 2 summarizes the material models used for the various solar cell laminating materials. Table 3 shows the geometric properties of the various layered materials used in solar PV cells.

Table 2. Solar cell material constitutive model.

Layer	Material	Constitutive Behaviour
Glass	Glass	Isotropic linear elastic
Encapsulant	Ethylene vinyl acetate (EVA)	Linear viscoelastic
Solar cell	Silicon	Anisotropic (different elastic constants at different loading directions)
Interconnector	Copper	Bi-linear (Young's modulus changes with temperature)
Busbar	Silver fingers	Isotropic linear elastic
Rear contact	Aluminum	Isotropic linear elastic
Interconnecting material	Solder ($Sn_{60}Pb_{40}$, $Sn_{3.8}Ag_{0.7}Cu$) IMC (Cu_3Sn, Ag_3Sn)	Solder: Generalized Garofalo–Arrhenius model IMCs: Isotropic linear elastic
Backsheet	Tedlar	Isotropic linear elastic

Table 3. The geometric properties of layer materials in solar PV cell.

Layer Material	Size (Length × Width)	Thickness (μm)	Reference
Glass	0.352 m × 0.156 m	3600	[22]
EVA	0.352 m × 0.156 m	450	[23]
Silicon	0.156 m × 0.156 m	175	[24]
Copper ribbons	0.156 m × 0.003 m	150	[12]
Solder	0.156 m × 0.003 m	20	[25–27]
IMC (Ag_3Sn, Cu_3Sn)	0.156 m × 0.003 m	4	[28–30]
Aluminum rear contact	0.156 m × 0.156 m	25	[14]
Silver (Ag) busbars	0.156 m × 0.003 m	50	[31]
Tedlar backsheet	0.352 m × 0.156 m	175	[32,33]

The creep behavior of solders was studied using the generalized Garofalo-Arrhenius model. Intermetallic compounds (IMCs) with a thickness of 6 μm, comprising Cu_3Sn_5 and Ag_3Sn on either side of the solder material, were used to completely model the interconnection. For the characterization of solder alloys, the Garofalo-Arrhenius model [34], using accumulated creep strain and dissipated strain energy density, which has an exponential dependence on temperature and a hyperbolic sine dependence on high stress, is commonly accepted. The flow equation for creep strain rate is given by:

$$\dot{\varepsilon}_{cr=C_1[\sinh(C_2\sigma)]^{C_3}exp}\left(\frac{-C_4}{T}\right) \quad (1)$$

where $\dot{\varepsilon}_{cr}$, σ and T are the scalar creep strain rate, von Mises effective stress and absolute temperature, respectively.

The other symbols (C_1, C_2, C_3 and C_4) represent material-dependent parameters. This model is used in this study to formulate the creep response of the solders and IMCs. Table 4 lists the various creep parameters used in predicting the thermo-mechanical response of the solders.

Table 4. Creep parameters for Garofalo–Arrhenius model.

Solder Material	C_1 (1/s)	C_2 $(MPa)^{-1}$	C_3	C_4	Reference
$Sn_{3.8}Ag_{0.7}Cu$	2.78×10^5	2.45×10^{-8}	6.41	6500	[19,35]
$Sn_{60}Pb_{40}$	$\frac{926 \times (508 - \theta)}{\theta}$	$\frac{1}{37.78 \times 10^6 - 74414 \times \theta}$ θ is the temperature in Kelvin	3.3	6360	[36]

For the analysis of each form of solder interconnection, four geometric models were developed. The ANSYS mesh development engine was used to mesh a sliced geometric model (quarter cell) (ANSYS Mesher). This engine discretizes the geometric model, making it possible to solve equations at nodal points. Refinement and sizing for high solution gradients and fine geometric details increased mesh performance and accuracy. The intermetallic compounds (IMCs) and solder geometric models were subjected to selective mesh adjustment and refinement operations in this study. The IMC, which is very thin (6μm), was subjected to ANSYS mesh refinement settings, while the solder geometric models were subjected to a face sizing environment. The model was used to create a mesh with a medium span angle center and minimum edge length using a device default size of mesh elements with an adaptive size feature and a medium relevance core. The resulting mesh statistics consisted of 195,329 nodes and 49,075 elements. The behavior of the soldered interconnection was studied in this analysis under thermal loads and boundary conditions from the 2012, 2013, 2014 and TRA thermal cycles. The aim of the analysis was to see

how the thermal loads and boundary conditions of different thermal cycles affected the creep damage in soldered interconnections. The equivalent von-Mises stress, equivalent creep strain distribution and response and the accumulated creep energy density (ACED) distribution over the 12 thermal cycles were evaluated.

2.4. Finite Element Model Validation of Solar Cell

The finite element model was validated by comparing the finite element simulation results from the ACED with results from experimental studies. Syed's [37] updated life prediction model was used to predict the life of the solder interconnections. Syed's model is based on creep strain energy density, which relates to the deformation stored internally throughout the volume of the joint during thermal loading.

This model offers a more robust damage indicator in the solder joint since creep strain energy density captures the entire deformation in the joint.

In this section, the authors predict the life of the solder interconnects using the accumulated creep energy density per cycle (W_{acc}) in Syed's [37] updated life prediction model given by:

$$N_f = (0.0069 W_{acc})^{-1} \tag{2}$$

In practice, the change in accumulated creep energy density per cycle (ΔW_{acc}) averaged over the volume of solder is used for predicting the cycles of failure. The (ΔW_{acc}) is obtained by computing the average change in creep energy density (ΔW_{ave}) from the finite element analysis (FEA) results and then normalized with the volume of the solder used in generating the geometric model. Thus,

$$\Delta W_{ave} = \frac{\sum_i^n W_2^i V_2^i}{\sum_i^n V_2^i} - \frac{\sum_i^n W_1^i V_1^i}{\sum_i^n V_1^i} \tag{3}$$

where W_2^i, W_1^i is the total ACED in one element at the end and the starting point of one thermal cycle, respectively. V_2^i, V_1^i is the volume of the element at the end and starting point of one cycle, respectively, and n is the number of selected elements used. The accumulated creep energy density per cycle (W_{acc}) is computed from the relation:

$$W_{acc} = \frac{\sum_{C_1}^{C_n} \Delta W_{acc}}{C_n} \tag{4}$$

where C_1 is the cycle number for the first thermal cycle, and C_n is the cycle number for the nth thermal cycle. For this study involving 12 thermal cycles: C_1 = 1 and C_n = 12.

Thus, we have

$$W_{acc} = \frac{\sum_1^{12} \Delta W_{acc}}{12} \tag{5}$$

The cycle time used in this study is 86,400 s (24 h or 1 day). Additionally, [38] reported that, within a temperature change of around 50 °C, PV modules generally experience one and a half (1.5) thermal cycles per day. Thus, the expected life (L_{years}) of interconnects (in years) is evaluated as:

$$L_{years} = \frac{\left(\frac{N_f}{1.5}\right)}{365} \tag{6}$$

Table 5 presents the results from the evaluation of W_{acc}, N_f and L_{years} from Equations (4)–(6), respectively.

Table 5. Expected life of solder interconnects from outdoor module (TRA) temperature cycle profile.

Solder Material	$Sn_{60}Pb_{40}$ (Tin-Lead)
Accumulated creep energy density per cycle (W_{acc})/(MJ/m^3)	0.01131
Expected life (N_f)/cycles	12,814
Expected life (L_{years})/years	23.4

According to Table 5, the findings of the life prediction analysis are very similar to those of Guyenot et al. [38], who estimated the life of PV modules operating per day with an average temperature gradient of around 50 °C to be 13,688 cycles (25 years). Furthermore, the findings are consistent with those of Köhl et al. [39], who recorded 10,950 cycles in a four-year German project. Kumar and Sakar [40] recorded a minimum life of 11,497 cycles (21 years) in a constant stress accelerated life test on 20 PV modules for stress-related failure, which closely matches the findings of this research. The results from the reported experimental studies undoubtedly validate the geometric model in this work. Subsequently, the finite element model was adopted for the study on creep damage in the soldered interconnections.

3. Results and Discussion

Damage to the solder caused by von-Mises equivalent stress, equivalent creep strain, accumulated creep strain and accumulated creep energy density is discussed in this section.

3.1. Study on Von-Mises Equivalent Stress of Solder Joint

Figure 5 displays the contour plots of equivalent von-Mises stress distribution (after 12 thermal cycles) in the solder interconnector joining the copper ribbon to the silver busbars on the solar cell. From the stress distribution in Figure 6, it is observed that the equivalent von-Mises stresses generated in the SnPb solder interconnection are generally higher than the stresses generated in the Pb-free solder interconnection for all four (4) different thermal cycles simulated in this study. The position of maximum and minimum stresses remained largely unchanged and was found to be closer to the cell gap region, where the copper ribbon bends over to connect the adjacent cell (front-to-back interconnection). From the TRA thermal cycle loading, a reduction of 2.2% in equivalent stress (from 8.7004 MPa to 8.5092 MPa) was observed when a SnPb solder was replaced with a Pb-free ($Sn_{3.8}Ag_{0.7}Cu$) solder interconnector. A reduction of 2.5% (from 9.0148 MPa to 8.7814 MPa) in equivalent stress from the SnPb solder to Pb-free solder interconnector was observed for the 2012 thermal cycle load profile. Furthermore, in a similar distribution for the years 2013 and 2014 (not displayed), a higher reduction of 6.7% (from 8.4852 MPa to 7.9169 MPa) in equivalent stress from a PbSn solder interconnector to a Pb-free solder interconnector was observed for the year 2013 thermal cycle. The results are summarized and presented in Table 6.

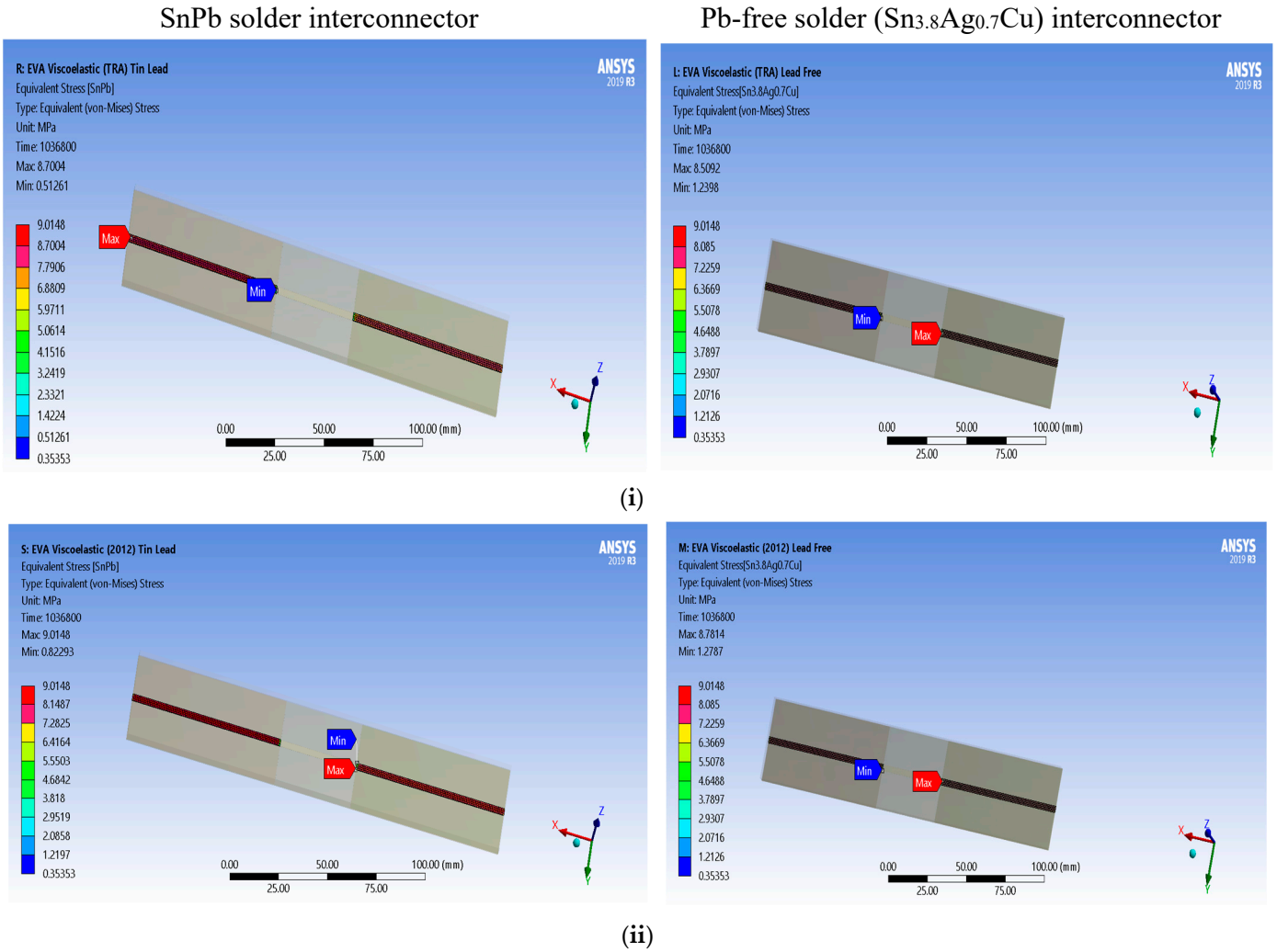

Figure 5. Equivalent von-Mises stress distribution on PbSn solder and Pb-free ($Sn_{3.8}Ag_{0.7}Cu$) solder for: (**i**) TRA and (**ii**) 2012 thermal cycles.

Table 6. Maximum equivalent von-Mises stress (MPa).

Thermal Cycles	TRA	2012	2013	2014
Tin-lead	8.7004	9.0148	8.4852	8.3618
Lead-free	8.5092	8.7814	7.9169	8.085
Change/%	2.2	2.5	6.7	3.3

Figure 6 depicts the stress response in soldered interconnections for the four thermal cycle profiles created from real-time monitoring of installed PV modules at the test site over a period of 12 cycles.

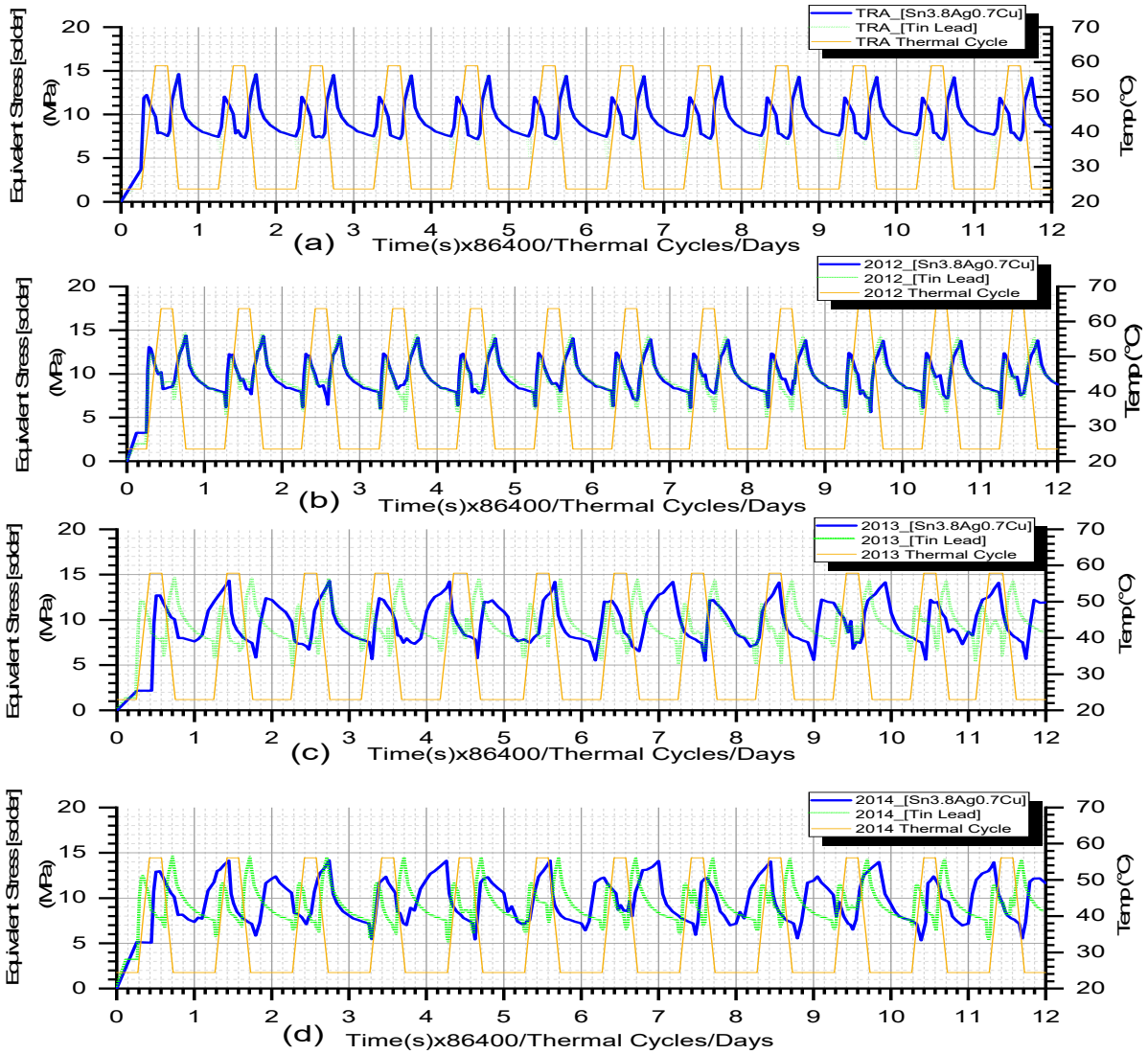

Figure 6. Equivalent von-Mises stress response of SnPb solder and Pb-free ($Sn_{3.8}Ag_{0.7}Cu$) solder for: (**a**) TRA, (**b**) 2012, (**c**) 2013 and (**d**) 2014 thermal cycles.

The equivalent von-Mises stress response in the solder over the 12 thermal cycles (TRA, 2012, 2013 and 2014 thermal cycles) presented in Figure 6 shows that, for both the SnPb and the Pb-free solders, the stresses rise to a peak value at a quarter-way through the first ramp-up step. Subsequently, the solders experience a gradual reduction in the equivalent stress as the heating progresses to a maximum cycle temperature (at the end of the first ramp-up). Generally, it was observed that the stresses generated in both solders show a near-constant amplitude (10 MPa) per cycle for the four different thermal cycles. From the TRA and 2012 thermal cycle profiles, the stresses in the two different solder alloys appear to track each over the 12 cycles.

This shows that the equivalent stresses developed in the solders remain the same for each time step. However, in the case of the 2013 and 2014 thermal cycle profiles, the response of the Pb-free solder appears to be out-of-phase with that of the SnPb solder. Whilst the SnPb solder shows a consistent response across the four different thermal cycle profiles under this study, the Pb-free solder appears to display sensitivity to the 2013 and 2014 thermal cycles. In the next section, the solder interconnections' responses to creep strain will be studied.

3.2. Study on Equivalent Creep Strain of Solder Joint

Creep strain affects the reliability of soldered interconnections in the solar PV module. In this study, we assessed the impact of the two types of solders (SnPb and $Sn_{3.8}Ag_{0.7}Cu$ (Pb-free)). Creep damage distributions are depicted in Figures 7 and 8 on the two types of solders of the modeled quarter symmetry of the front-to-back solar cell interconnection subjected to the four different temperature load profiles (TRA, 2012, 2013, 2014).

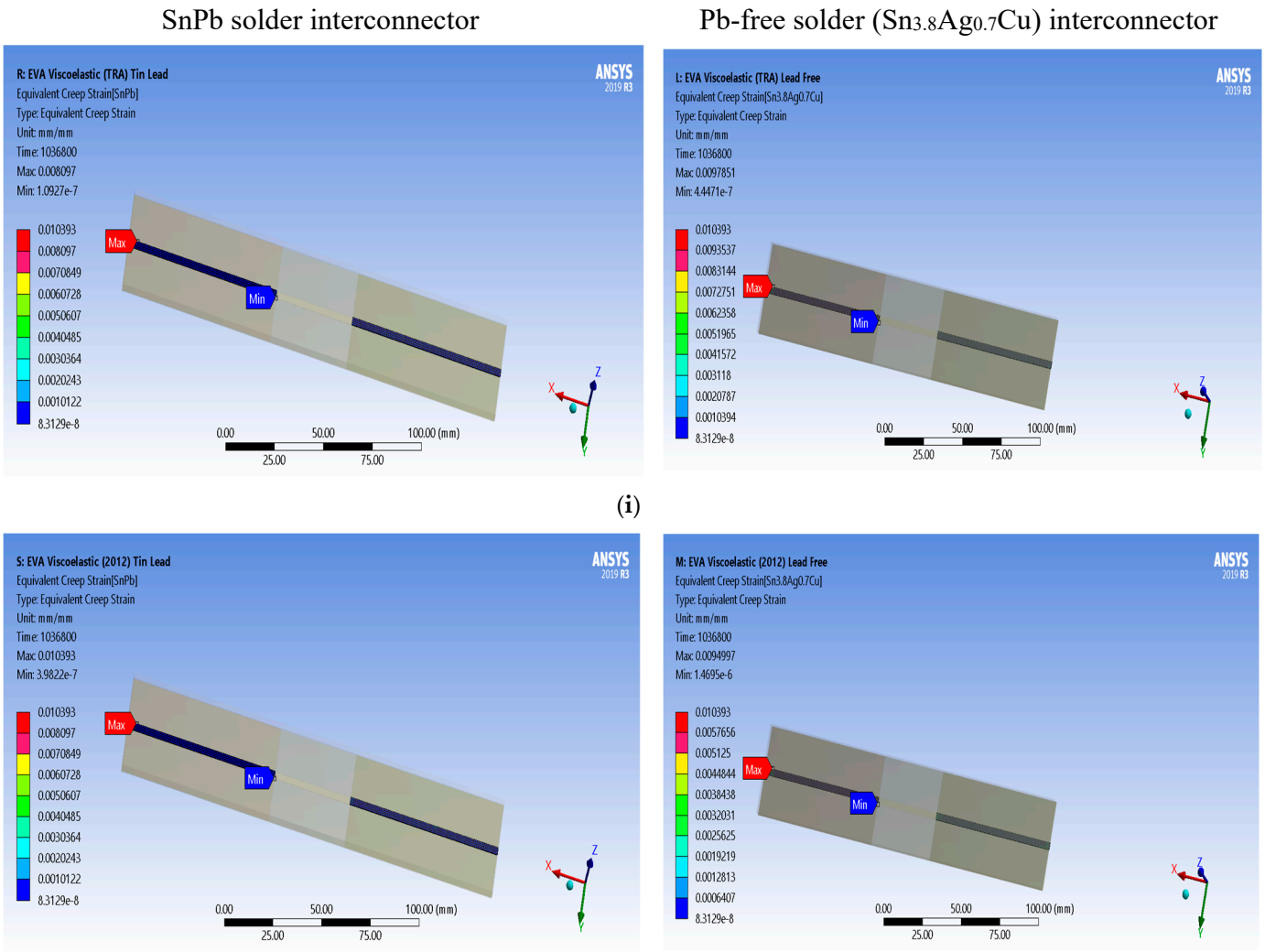

Figure 7. Equivalent creep strain distribution on PbSn solder and Pb-free ($Sn_{3.8}Ag_{0.7}Cu$) solder for: (**i**) TRA, (**ii**) 2012 thermal cycles.

From Figures 7 and 8, a decrease in equivalent creep strain can be observed for the 2012, 2013 and 2014 thermal cycles when the interconnecting solder is changed from a SnPb to a Pb-free solder. However, an increase in equivalent creep strain was observed when the solder was changed from the SnPb to Pb-free solder under the TRA thermal cycle. Thus, the solder materials display some sensitivity to the thermal cycle parameters.

The results of the creep strain distribution in Figure 9 indicate that when the SnPb solder interconnector is substituted with a Pb-free interconnector the creep strain decreases slightly at the end of twelve thermal cycles in 2012, 2013 and 2014. The TRA thermal cycle, on the other hand, shows a large increase in equivalent creep strain (around 20%) when the SnPb is replaced with Pb-free solder.

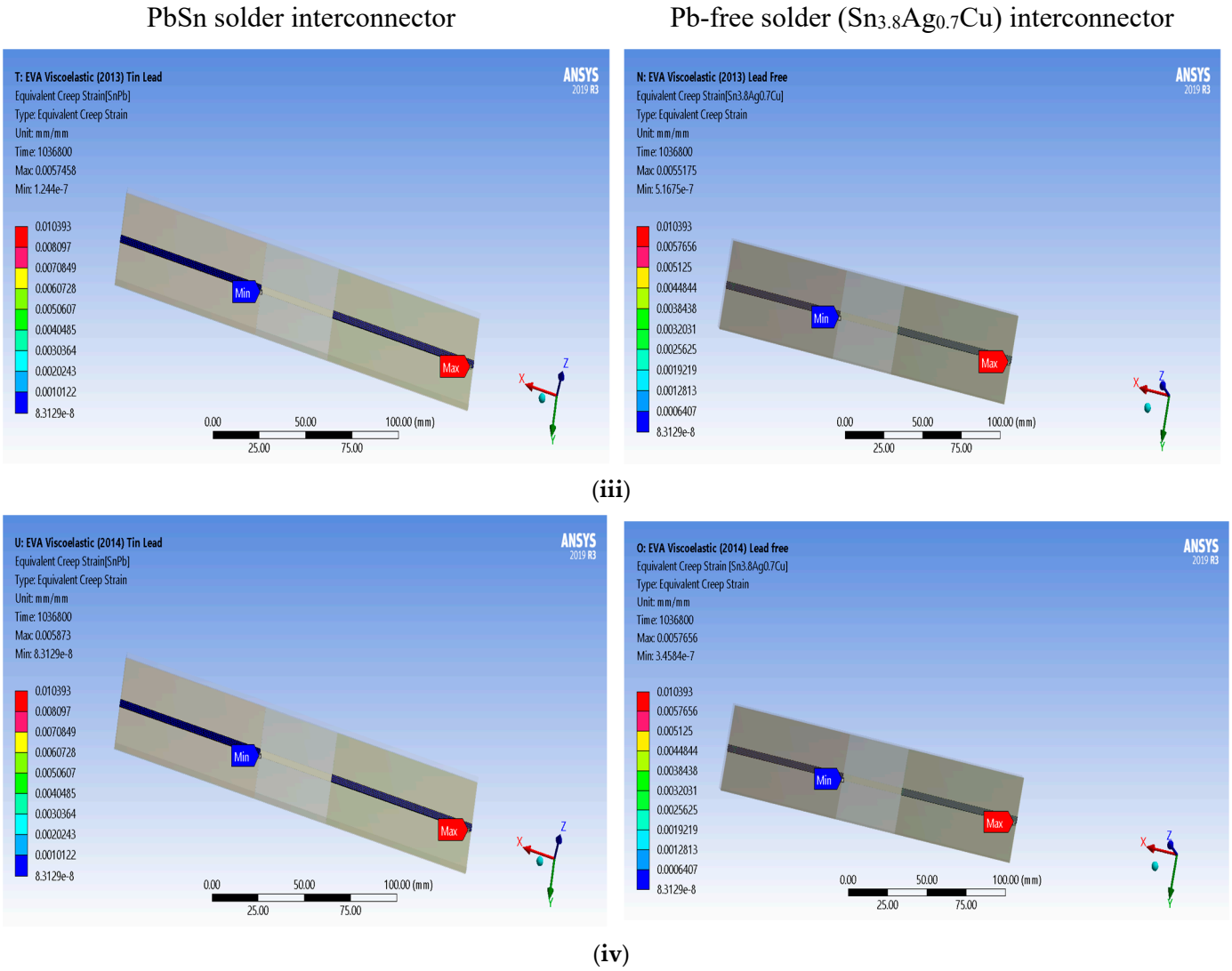

Figure 8. Equivalent creep strain distribution on PbSn solder and Pb-free ($Sn_{3.8}Ag_{0.7}Cu$) solder for: (**iii**) 2013 and (**iv**) 2014 thermal cycles.

Figure 9 shows the variation in the creep strain induced in the solder interconnectors over the thermal cycles. The creep strain responses from the respective thermal cycles (TRA, 2012, 2013 and 2014 thermal cycles) were superimposed onto one another. It can also be observed from Figure 9 that the creep strain profiles in both the Pb-Sn solder and Pb-free solder vary with approximately equal amplitude per cycle (closely tracking each other over the 12 cycles) for the 2013 and 2014 thermal cycles. With the TRA thermal cycle, the creep strain responses of the two solders appear to track each other, with approximately equal creep strain amplitude up to the fourth (4th) thermal cycle.

Subsequently, the Pb-free solder experiences a higher increase in creep strain per cycle compared with the SnPb solder. However, with the 2012 thermal cycle, a marked difference in the creep strain responses of the two solders was observed after the first (1st) thermal cycle. Furthermore, a higher increase in creep strain per cycle was registered in the SnPb compared with the Pb-free solder. These preliminary results indicate that Pb-free solder is a good substitute for the SnPb solder in the manufacturing of solar PVs.

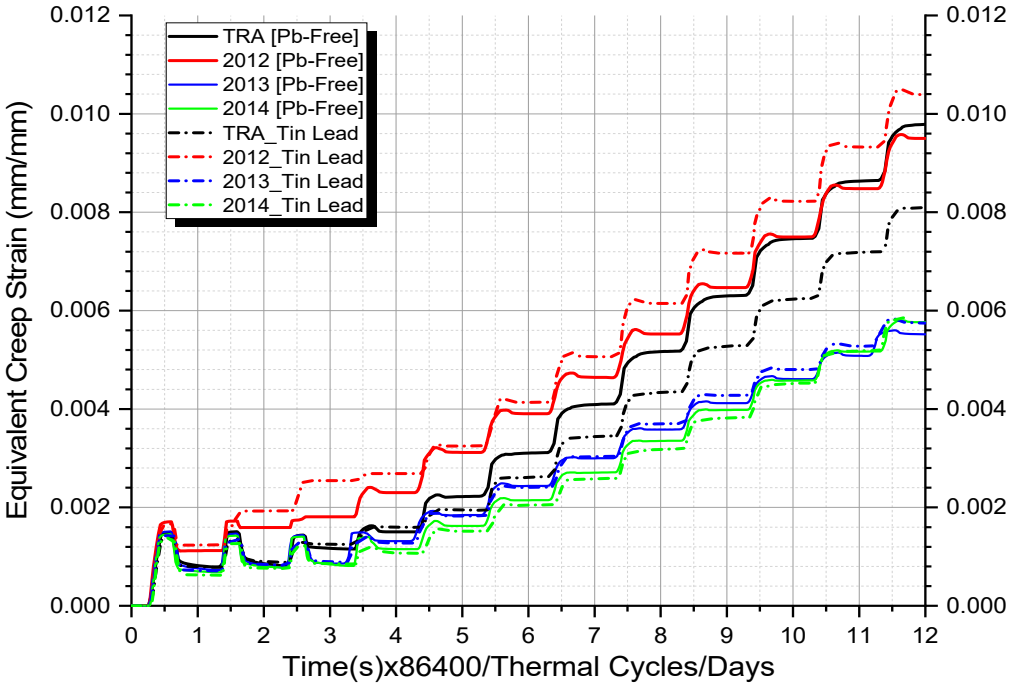

Figure 9. Superimposed plots of equivalent creep Strain versus Thermal Cycles.

The outputs of the creep strain response curves over the different thermal cycles show that creep damage is sensitive to the thermal cycle parameters. Overall, the 2012 thermal cycle imposed the maximum creep damage of 0.010393 m/m on the SnPb solder interconnection, whilst the 2013 thermal cycle imposed the minimum creep damage of 0.0057458 m/m on the SnPb solder interconnection. In the case of the Pb-free solder interconnection, the TRA thermal cycle imposed the maximum creep damage of 0.009785 m/m, whilst the 2013 thermal cycle imposed the minimum creep damage of 0.0055175 m/m. Although creep strain indicates damage in the solder interconnection, there exist superior damage indicators, such as accumulated creep strain and accumulated creep energy density, which can analyze the damage quantitatively. The accumulated creep strain damage is discussed in the next section.

3.3. Evaluation of Accumulated Creep Strain in Solder Interconnections

Apart from the energy density methods (strain energy density and creep energy density), the accumulated creep strain (ε_{acc}) remains one of the key life prediction parameters. The distributions of accumulated creep strain at the end of 12 thermal cycles are depicted in Figures 10 and 11. The accumulated creep strain is evaluated using the SEND CREEP command NLCREQ in Ansys. In this study, the accumulated creep strain damage in the two different solder interconnections (PbSn and $Sn_{3.8}Ag_{0.7}Cu$ (Pb-free)) for the temperature load cycles (2012, 2013, 2014 and TRA thermal cycles) was evaluated. Results from the distribution in Figures 10 and 11 show that for all the temperature cycles investigated, the accumulated creep strain generated in the Pb-free solder interconnection was found to be higher than that in the SnPb solder interconnection.

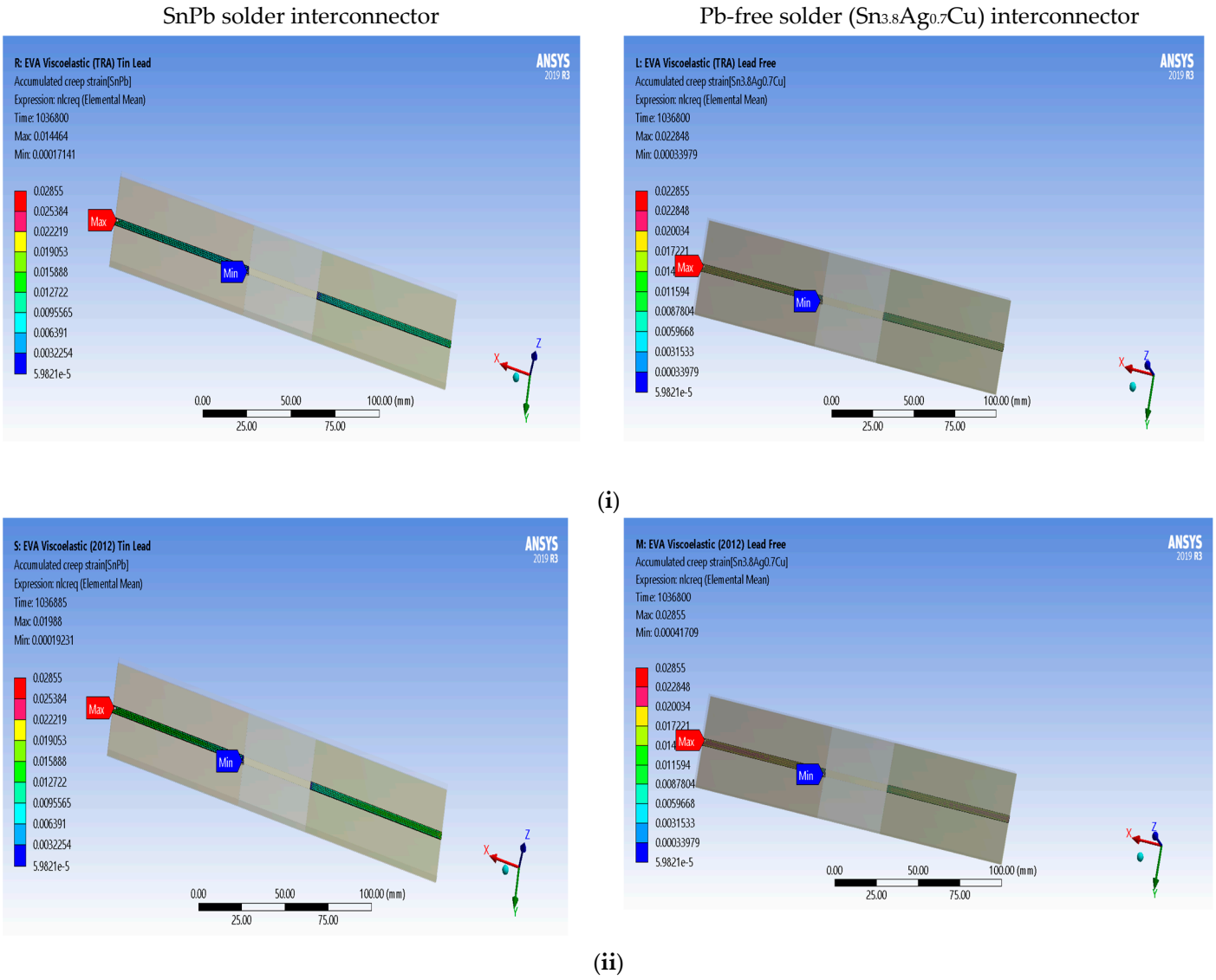

Figure 10. Accumulated creep strain damage distribution in PbSn and Pb-free solder interconnection for: (**i**) TRA and (**ii**) 2012 thermal cycles.

A maximum accumulated creep strain damage of 0.028555 mm/mm was generated in the Pb-free solder interconnection during the 2012 thermal load cycle (Figure 10ii) and the minimum accumulated creep strain of 0.012002 mm/mm (Figure 11ii) in the SnPb solder interconnection during the 2014 thermal load cycle. Overall, the 2012 thermal cycle induced the maximum accumulated creep strain in both interconnections (0.01988 mm/mm for SnPb solder and 0.028555 mm/mm for Pb-free).

Table 7 presents a summary of the percentage change in accumulated creep strain from the SnPb solder interconnection to the Pb-free solder interconnection. It was observed that for the 2012, 2013 and 2014 thermal cycles, the accumulated creep strain damage increases by an average value of 45% when the interconnection solder is changed from an SnPb solder to Pb-free solder. However, the increase in accumulated creep strain was lower than the 57.96% increase resulting from the TRA cycle. The value of 57.96% must be the true value for the test region since it uses the average of the temperature load data from 2012–2014, as previously indicated.

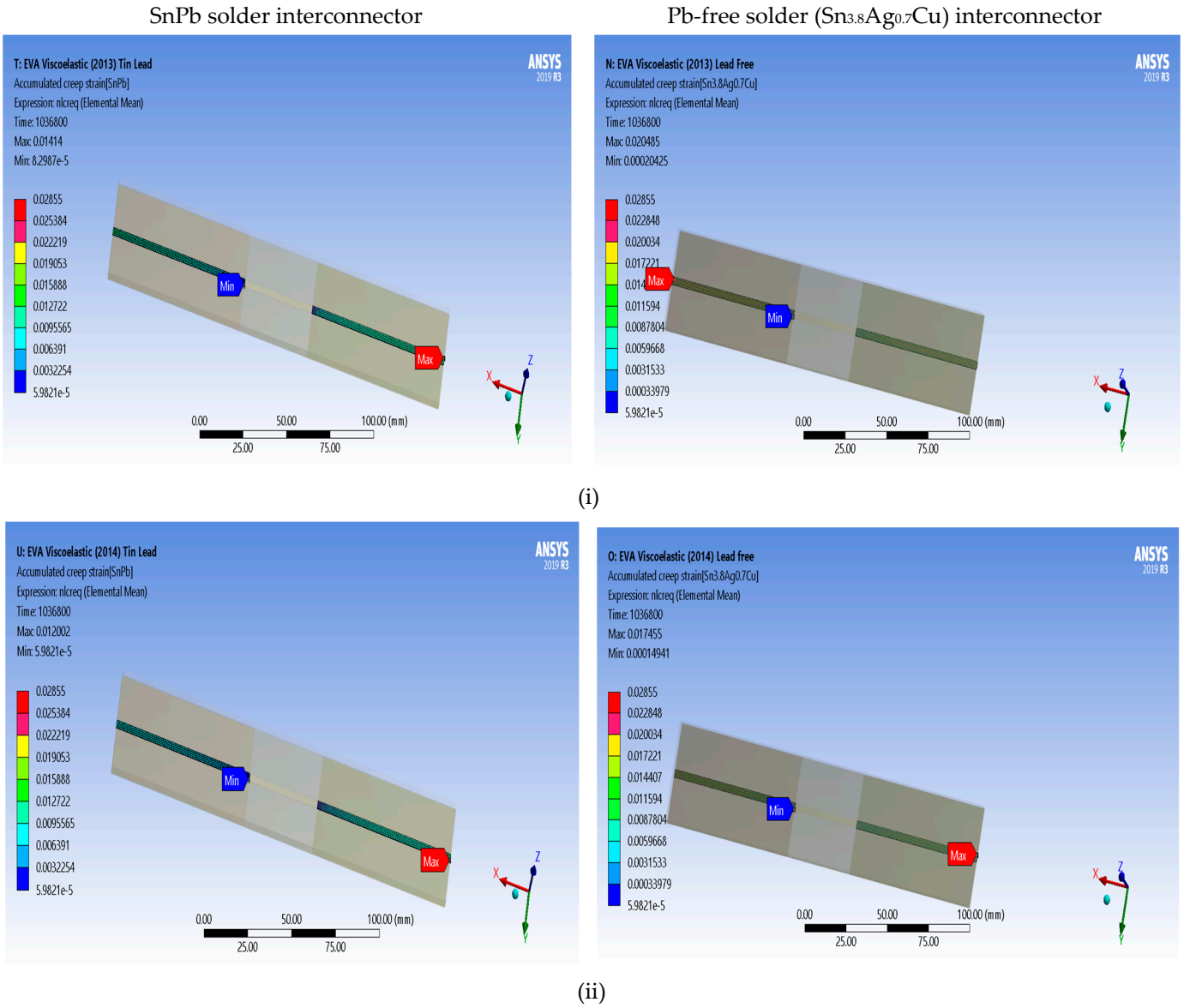

Figure 11. Accumulated creep strain damage distribution in PbSn and Pb-free solder interconnect for (**i**) 2013 and (**ii**) 2014 thermal cycles.

Table 7. Percentage change in accumulated creep strain.

Thermal Cycles		TRA	2012	2013	2014
Accumulated creep strain (ε_{acc}) (mm/mm)	SnPb-solder	0.014464	0.01988	0.01414	0.012002
	$Sn_{3.8}Ag_{0.7}Cu$	0.022848	0.02855	0.020485	0.017455
Change in accumulated creep strain %		57.96%	43.61%	44.87%	45.43%

Displayed in Figure 12 is the accumulated creep strain response over the 12 thermal cycles. The response of accumulated creep strain over the 12 thermal cycles presented in Figure 12 shows that, for up to the third thermal cycle, the accumulated creep strain damage response in the Pb-free solder interconnection remained largely unchanged for the 2013, 2014 and TRA cycles.

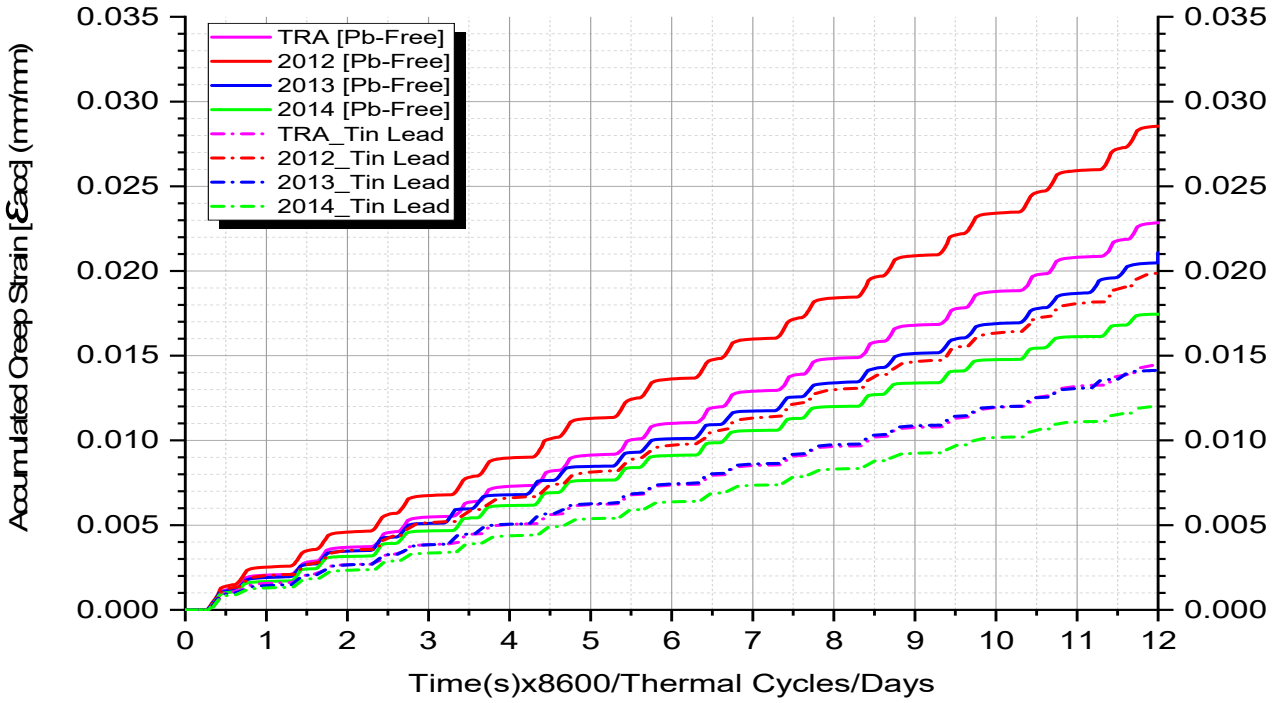

Figure 12. Accumulated creep strain response for PbSn and Pb-free solder for: TRA, 2012, 2013 and 2014 thermal cycles.

After the third thermal cycle, however, variations in the cumulative creep strain response become more pronounced. The damage accumulation in the Pb-free solder for the 2013 and 2014 thermal cycles was slightly lower than during the TRA thermal period at the end of the 12 thermal cycles. The cumulative creep strain damage per cycle from the 2012 thermal cycle was found to be higher than that of the TRA thermal cycle, while using the same Pb-free solder interconnection. Similarly, for the 2013, 2014 and TRA periods, the cumulative creep damage response remained roughly equal up to the second thermal cycle with the SnPb solder interconnection. This trend continued with the 2013 and TRA cycles, which remain unchanged until the end of the 12 thermal cycles. However, the accumulated creep strain responses for the 2014 thermal cycle produced a relatively lower accumulated creep strain per cycle after the second thermal cycle and until the end of the 12 thermal cycles. This observation confirms what has been reported previously by Amalu and Ekere [41], who observed that, for a given thermal loading cycle, more than three thermal cycles are required to effectively assess creep damage in solders. Fewer than four thermal cycles may generate misleading results. It was observed further that the 2012 thermal cycle generated a relatively higher creep strain damage per cycle in the SnPb solder interconnection. The results from the accumulated creep strain show that the fatigue life of Pb-free solder interconnections is expected to be relatively lower as compared with SnPb solder interconnects at the test site. However, Syed [37] observed that the accumulated creep strain displays sensitivity to the type of constitutive equation used in modeling the behavior of the solder joint. Additionally, the accumulated creep strain is unable to capture damage resulting from low-temperature dwells effectively. On the other hand, the accumulated creep energy density (W_{acc}) parameter can capture the damage from low-temperature dwells and does not display noticeable sensitivity to the constitutive model of the solder. Thus, the accumulated creep energy density offers a comparatively better parameter for fatigue life prediction in solder joints. In the next section, the accumulated creep energy density in the solder interconnections generated by the thermal cycles is evaluated.

3.4. Evaluation of Accumulated Creep Energy Density (ACED) in Solder Interconnections

In Section 3.4, the cumulative creep energy density (ACED) was determined for the 2012, 2013, 2014 and TRA thermal cycles in Ansys using the creep work command NL CRWK. Figure 13 summarizes and describes the ACED distributions at the end of 12 thermal cycles.

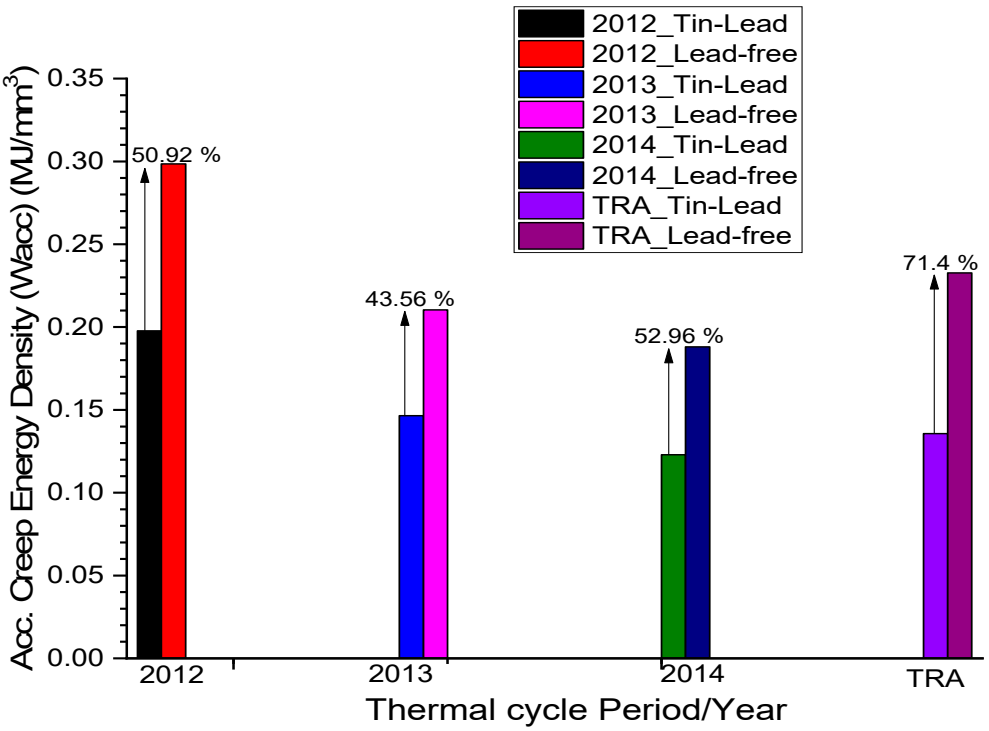

Figure 13. Column distribution of accumulated creep energy density for 2012, 2013, 2014 and TRA thermal cycles.

Figure 13 shows a column plot of cumulative creep energy density for the four thermal cycle profiles at the end of 12 thermal cycles. During the TRA thermal cycle, replacing the SnPb solder with a Pb-free solder interconnection resulted in a maximum percentage change of 71.4% (from 1.3573 $\times$ 10^5 J/mm^3 to 2.3275 $\times$ 10^5 J/mm^3) in accumulated creep energy density. The 2013 thermal cycle, on the other hand, saw a minimum change in cumulative creep strain energy density of 43.56%. As a result, the TRA thermal cycle has a higher sensitivity to solder interconnection material properties than the 2013 thermal cycle, which has a lower sensitivity to solder interconnection material properties.

Figure 14 shows the time-dependent cumulative creep energy density for the two separate solder interconnection materials over various thermal cycle profiles. The accumulated creep energy density profiles for 2013 and TRA thermal cycles remained roughly similar for up to six thermal cycles with the Pb-free solder interconnection, as shown in Figure 14. The accumulated creep energy density profiles for 2013 and TRA for the SnPb solder interconnection remained the same for up to the third thermal period. Furthermore, the ACED profile produced in the Pb-free interconnection during the TRA cycle shows a higher ACED per cycle from the sixth to the end of the 12th thermal cycle than the 2013 cycle. In comparison, the ACED profile for the TRA thermal cycle produced in the SnPb solder interconnection shows a lower ACED than the 2013 thermal cycle after the third thermal cycle. The findings show that more than six thermal cycles are needed to accurately measure ACED damage in the solder interconnection.

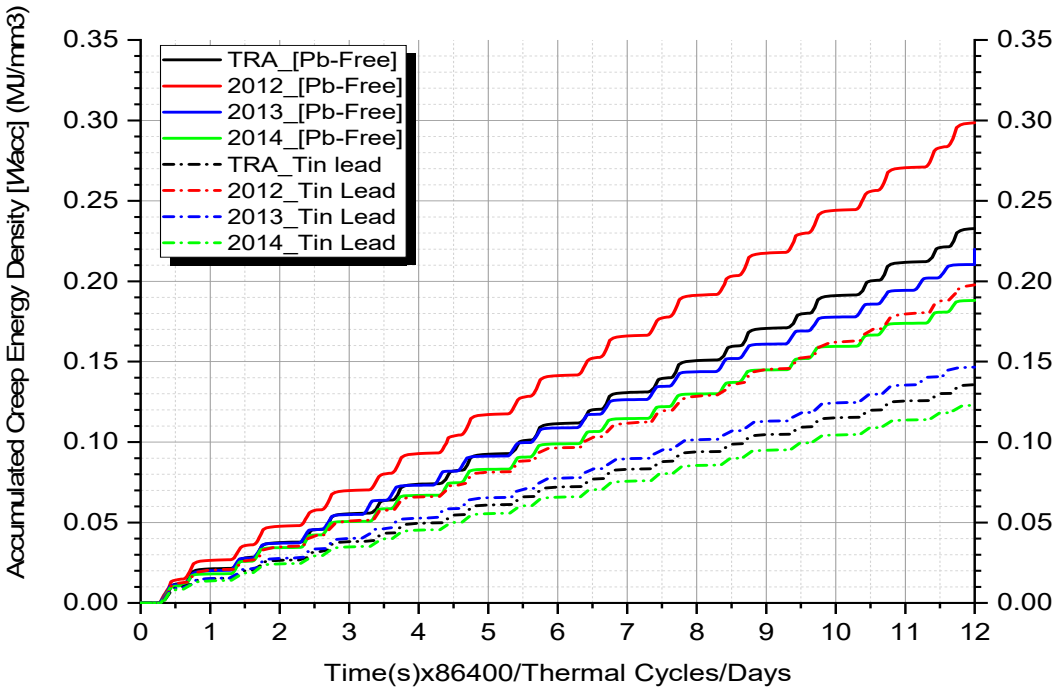

Figure 14. Accumulated creep energy density (ACED) response over 12 thermal cycles for: TRA, 2012, 2013 and 2014 thermal cycles.

4. Conclusions

The creep damage of the solder interconnection in a solar PV is evaluated in this study for both SnPb and Pb-free solders. For the years 2012, 2013 and 2014, the study used thermal cycle loads produced by real-time monitoring of module temperatures on installed PV modules. This research also made use of a test area average (TRA) thermal cycle established in a previous study. The 2012 thermal cycle caused maximum stress and creep strain damage of 9.0148 MPa and 0.010393 m/m, according to the results of the numerical analysis. The maximum stress and creep strain in the SnPb solder interconnection were measured. During the 2013 thermal cycle, the minimum equivalent stress and creep strain damage in the Pb-free solder interconnection were 7.9169 MPa and 0.0055175 m/m, respectively. The Pb-free solder interconnection accrued the most creep strain damage during the 2012, 2013 and 2014 thermal cycles, according to the accumulated creep strain results. The average percentage change in cumulative creep damage obtained by replacing the SnPb solder interconnection with a Pb-free solder was found to be approximately 45% over these three thermal cycles. Under the TRA thermal cycle, the change in cumulative creep strain was found to be higher when the SnPb solder interconnection was substituted with a Pb-free solder (57.96%). During the TRA thermal cycle, the SnPb solder was replaced with a Pb-free solder interconnection, resulting in a maximum percentage change of 71.4% in accumulated creep energy density. At the KNUST test site in Kumasi, Ghana, this study found that Sn60Pb40 solder interconnections are likely to be more reliable than Sn3.8Ag0.7Cu (Pb-free) solder interconnections. To predict damage in soldered interconnections, the analysis can be replicated at different test sites.

Author Contributions: G.T. (Project Manager- Provided direction of research, resources, supervision, conceptualization, methodology, review-editing); F.K.A.N.-PhD Student (carried out FE Modelling using Ansys software, validation analysis, write-up); F.B.E. (Contributed to the FE Modelling using Ansys software, investigation and part of the write-up). All authors have read and agreed to the published version of the manuscript.

Funding: This research work was carried out with technical and financial support from Arizona State University Photovoltaic Reliability Laboratory, USA, USAID/NAS and Norwegian Government (NORAD for the EnPe Project). These supports ended in 2018. The APC was funded by Prof. Gabriel Takyi (The manager of the research work).

Data Availability Statement: Some or all data, models, or code that support the findings of this study are available from the corresponding author upon reasonable request.

Acknowledgments: The authors acknowledge the financial support received from the USAID for the PRESSA project, sub-grant no. 2000004829, through the US National Academy of Sciences. The authors appreciate the technical support provided by Dr Mani and Sai Tatapudi from the Arizona State University Photovoltaic Reliability Laboratory (PRL). The authors also acknowledge the support received from the Norwegian Programme for Capacity Development in Higher Education and Research for Development within the Fields of Energy and Petroleum (EnPE), and The Brew-Hammond Energy Center (TBHEC), KNUST, Ghana.

Conflicts of Interest: The authors would like to state that there are no conflicts of interest situation regarding any aspect of this research work.

References

1. Al-Khori, K.; Bicer, Y.; Koç, M. Comparative techno-economic assessment of integrated PV-SOFC and PV-Battery hybrid system for natural gas processing plants. *Energy* **2021**, *222*, 119923. [CrossRef]
2. Zhang, J. Solar PV Market Research and Industry Competition Report. *IOP Conf. Ser. Earth Environ. Sci.* **2021**, *632*, 032047. [CrossRef]
3. King, D.L.; Boyson, W.E.; Kratochvil, J.A. *Photovoltaic Array Performance Model*; Sandia Report; Sandia National Laboratories: Albuquerque, NM, USA, 2004.
4. Clech, J.-P. Acceleration factors and thermal cycling test efficiency for lead-free Sn-Ag-Cu assemblies. In Proceedings of the SMTA International Conference, Chicago, IL, USA, 25–29 September 2005; pp. 902–917.
5. Aberle, A.G.; Wenham, S.R.; Green, M.A. A new method for accurate measurements of the lumped series resistance of solar cells. In Proceedings of the Twenty Third IEEE Photovoltaic Specialists Conference—1993 (Cat. No.93CH3283-9), Louisville, KY, USA, 10–14 May 1993; pp. 133–139.
6. Van Dyk, E.E.; Meyer, E.L. Analysis of the effect of parasitic resistances on the performance of photovoltaic modules. *Renew. Energy* **2004**, *29*, 333–344. [CrossRef]
7. Tien, J.K.; Hendrix, B.C.; Bretz, P.L.; Attarwala, A.I. Creep-fatigue interactions in solders. In Proceedings of the 39th Electronic Components Conference, Houston, TX, USA, 22–24 May 1989; Volume 12, pp. 502–505. [CrossRef]
8. Hasan, O.; Arif, A.F.M. Performance and life prediction model for photovoltaic modules: Effect of encapsulant constitutive behavior. *Sol. Energy Mater. Sol. Cells* **2014**, *122*, 75–87. [CrossRef]
9. Kraemer, F.; Wiese, S. FEM stress analysis of various solar module concepts under temperature cycling load. In Proceedings of the 2014 15th International Conference on Thermal, Mechanical and Mulit-Physics Simulation and Experiments in Microelectronics and Microsystems (EuroSimE), Ghent, Belgium, 7–9 April 2014; pp. 1–8.
10. Lee, Y.; Tay, A.A. Finite Element Thermal Analysis of a Solar Photovoltaic Module. *Energy Procedia* **2012**, *15*, 413–420. [CrossRef]
11. Dietrich, S.; Pander, M.; Sander, M.; Schulze, S.H.; Ebert, M. Mechanical and thermomechanical assessment of encapsulated solar cells by finite-element-simulation. *Reliab. Photovolt. Cells Modul. Compon. Syst. III* **2010**, *773*, 77730F.
12. Wiese, S.; Meier, R.; Kraemer, F. Mechanical behaviour and fatigue of copper ribbons used as solar cell interconnectors. In Proceedings of the 2010 11th International Thermal, Mechanical & Multi-Physics Simulation, and Experiments in Microelectronics and Microsystems (EuroSimE), Bordeaux, France, 26–28 April 2010; pp. 1–5. [CrossRef]
13. Wiese, S.; Meier, R.; Kraemer, F.; Bagdahn, J. Constitutive behaviour of copper ribbons used in solar cell assembly processes. In Proceedings of the EuroSimE 2009—10th International Conference on Thermal, Mechanical and Multi-Physics Simulation and Experiments in Microelectronics and Microsystems, Delft, The Netherlands, 26–29 April 2009; pp. 1–8.
14. Chen, C.-H.; Lin, F.-M.; Hu, H.-T. and Yeh, F-Y. Residual stress and bow analysis for silicon solar cell induced by soldering. *Int. Symp. Sol. Cell Technol.* **2008**, 4–6.
15. Eitner, U.; Altermatt, P.P.; Kontges, M.; Meyer, R.; Brendel, R. A modeling approach to the optimization of interconnects for back contact cells by thermomechanical simulations of photovoltaic modules. In Proceedings of the 23rd European Photovoltaic Solar Energy Conference (EU PVSEC), Valencia, Spain, 1–5 September 2008; pp. 1–5.
16. Eitner, U.; Kajari-Schröder, S.; Köntges, M.; Altenbach, H. Thermal Stress and Strain of Solar Cells in Photovoltaic Modules. In *Shell-like Structer*; Springer: Berlin/Heidelberg, Germany, 2011; pp. 453–468.
17. Eitner, U.; Pander, M.; Kajari-Schröder, S.; Köntges, M.; Altenbach, H. Thermomechanics of PV modules including the viscoelasticity of EVA. In Proceedings of the 26th European Photovoltaic Solar Energy Conference and Exhibition, Hamberg, Germany, 5–9 September 2011; pp. 3267–3269.

18. Hasan, O.; Arif, A.F.M.; Siddiqui, M.U. Finite Element Modeling, Analysis, and Life Prediction of Photovoltaic Modules. *J. Sol. Energy Eng.* **2014**, *136*, 021022. [CrossRef]
19. Zarmai, M.; Ekere, N.N.; Oduoza, C.; Amalu, E.H. (Emeka) Optimization of thermo-mechanical reliability of solder joints in crystalline silicon solar cell assembly. *Microelectron. Reliab.* **2016**, *59*, 117–125. [CrossRef]
20. Nyarko, F.K.; Takyi, G.; Amalu, E.H.; Adaramola, M.S. Generating temperature cycle profile from in-situ climatic condition for accurate prediction of thermo-mechanical degradation of c-Si photovoltaic module. *Eng. Sci. Technol. Int. J.* **2019**, *22*, 502–514. [CrossRef]
21. Park, N.; Jeong, J.; Han, C. Estimation of the degradation rate of multi-crystalline silicon photovoltaic module under thermal cycling stress. *Microelectron. Reliab.* **2014**, *54*, 1562–1566. [CrossRef]
22. Willeke, G.P.; Weber, E.R. *Advances in Photovoltaics: Newnes*; Academic Press: Cambridge, MA, USA, 2013.
23. Cuddalorepatta, G.; Dasgupta, A.; Sealing, S.; Moyer, J.; Tolliver, T.; Loman, J. Durability of Pb-free solder between copper inter-connect and silicon in photovoltaic cells. *Prog. Photovolt. Res. Appl.* **2010**, *18*, 168–182. [CrossRef]
24. Saga, T. Advances in crystalline silicon solar cell technology for industrial mass production. *NPG Asia Mater.* **2010**, *2*, 96–102. [CrossRef]
25. Wirth, H. Lasers in Wafer-based PV Module Production. *Laser Tech. J.* **2010**, *7*, 36–38. [CrossRef]
26. Rogelj, I.; Ziger, P.; Eiselt, P. PV Ribbon design specification. Overview of Product specification and Comparison of production processes. SOLARCON. 2012. Available online: http://plasmait.com/wp-content/uploads/2015/01/SEMICON-China-2012-PV-Ribbon-Production.pdf (accessed on 15 April 2021).
27. Moyer, J.; Zhang, W.; Kurtz, E.; Tavares, R.; Buzby, D.; Kleinbach, S. The role of silver contact paste on reliable connectivity sys-tems. In Proceedings of the 25th European Photovoltaic Solar Energy Conference and Exhibition, Valencia, Spain, 6–10 September 2010.
28. Choi, W.K.; Jang, S.-Y.; Kim, J.H.; Paik, K.-W.; Lee, H.M. Grain Morphology of Intermetallic Compounds at Solder Joints. *J. Mater. Res.* **2002**, *17*, 597–599. [CrossRef]
29. Mei, Z.; Sunwoo, A.J.; Morris, J.W. Analysis of low-temperature intermetallic growth in copper-tin diffusion couples. *Metall. Trans. A* **1992**, *23*, 857–864. [CrossRef]
30. Prakash, K.; Sritharan, T. Interface reaction between copper and molten tin–lead solders. *Acta Mater.* **2001**, *49*, 2481–2489. [CrossRef]
31. Zemen, Y.; Teusch, H.; Kropke, G.; Pingel, S.; Held, S. The Impact of Busbar Surface Topology and Solar Cells Soldering Process. In Proceedings of the 27th European Photovoltaic Solar Energy Conference and Exhibition, Frankfurt, Germany, 24–28 September 2012; pp. 24–28.
32. Armstrong, S.; Hurley, W. A thermal model for photovoltaic panels under varying atmospheric conditions. *Appl. Therm. Eng.* **2010**, *30*, 1488–1495. [CrossRef]
33. Arangú, A.V.; Ponce-Alcántara, S.; Sánchez, G. Optical characterization of backsheets to improve the power of photovoltaic modules. In Proceedings of the 8th International Photovoltaic Power Generation Conference and Exhibition, SNEC, Shanghai, China, 20–22 May 2014; pp. 20–22.
34. Amalu, E.H.; Ekere, N. High-temperature fatigue life of flip chip lead-free solder joints at varying component stand-off height. *Microelectron. Reliab.* **2012**, *52*, 2982–2994. [CrossRef]
35. Amalu, E.H.; Ekere, N.N. Modelling evaluation of Garofalo-Arrhenius creep relation for lead-free solder joints in surface mount electronic component assemblies. *J. Manuf. Syst.* **2016**, *39*, 9–23. [CrossRef]
36. Deplanque, S.; Nuchter, W.; Spraul, M.; Wunderie, B.; Dudek, R.; Michel, B. Relevance of primary creep in thermo-mechanical cy-cling for life-time prediction in Sn-based solders. In Proceedings of the EuroSimE 2005 Proceedings of the 6th International Conference on Ther-mal, Mechanial and Multi-Physics Simulation and Experiments in Micro-Electronics and Micro-Systems, Berlin, Germany, 18–20 April 2005; pp. 71–78.
37. Syed, A. Updated Life Prediction Models for Solder Joints with Removal of Modeling Assumptions and Effect of Constitutive Equations. In Proceedings of the 7th International Conference on Thermal, Mechanical and Multiphysics Simulation and Experiments in Micro-Electronics and Micro-Systems, Chandler, AZ, USA, 24–26 April 2006; pp. 1–9.
38. Guyenot, M.; Peter, E.; Zerrer, P.; Kraemer, F.; Wiese, S. Enhancing the lifetime prediction methodology for photovoltaic modules based on electronic packaging experience. In Proceedings of the 2010 11th International Thermal, Mechanical & Multi-Physics Simulation, and Experiments in Microelectronics and Microsystems (EuroSimE), Linz, Austria, 18–20 April 2011. [CrossRef]
39. Köhl, M.; Weiss, K.; Heck, M.; Philipp, D. PV reliability: Results of a German four-year joint project Part I: Accelerated ageing tests and modelling of degradation. In Proceedings of the 24th European Photovoltaic Solar Energy Conference and Exhibition, Hamburg, Germany, 21–25 September 2009.
40. Kumar, S.; Sarkan, B. Design for reliability with weibull analysis for photovoltaic modules. *Int. J. Curr. Eng. Technol.* **2013**, *3*, 129–134.
41. Amalu, E.H.; Ekere, N.N. Damage of lead-free solder joints in flip chip assemblies subjected to high-temperature thermal cycling. *Comput. Mater. Sci.* **2012**, *65*, 470–484. [CrossRef]